Density Functional Calculations on Disaccharide Mimics: Studies of Molecular Geometries and Trans-*O*-glycosidic $^3J_{COCH}$ and $^3J_{COCC}$ Spin-Couplings

Francis Cloran,[†] Ian Carmichael,[‡] and Anthony S. Serianni*[,†]

Contribution from the Department of Chemistry and Biochemistry, and the Radiation Laboratory, University of Notre Dame, Notre Dame, Indiana 46556

Received December 21, 1998. Revised Manuscript Received April 22, 1999

Abstract: Density functional theory (DFT) using the B3LYP functional and the split-valence 6-31G* basis set has been used to investigate the structures and conformations of four β-[1→4]-linked disaccharide mimics, **1**−**4**. Systematic functional group substitution at sites near the glycosidic linkage was used to evaluate the effects of sterics and interresidue hydrogen bonding on the preferred glycosidic torsion angles ϕ and ψ. Using DFT-optimized geometries, the same hybrid functional, and a specially designed basis set, vicinal NMR scalar coupling constants involving carbon ($^3J_{COCH}$, $^3J_{COCC}$) across the glycosidic linkages of **1**−**4** were calculated as a function of the ϕ and ψ torsion angles, and the resulting torsional dependencies were compared to recently reported experimental Karplus curves for these coupling pathways (Bose, B.; et al. *J. Am. Chem. Soc.* **1998**, *120*, 11158−11173). The new computational data are in excellent agreement with experimental results and confirm the general shape of the experimental curves. For $^3J_{COCH}$, however, small discrepancies were observed at the extreme dihedral angles, suggesting some deficiencies in the theory and/or experimental data. For $^3J_{COCC}$, the new computed couplings confirm the existence of terminal electronegative substituent effects on coupling magnitude, and computed couplings in the 0−100° range of dihedral angles lead to an improved Karplus curve for the interpretation of $^3J_{COCC}$ values across the *O*-glycosidic linkages of oligosaccharides.

Introduction

A key objective of conformational studies of oligosaccharides in solution is the assessment of the torsional behavior of their constituent glycosidic linkages (Scheme 1), since these torsions largely determine overall shape or topology. The glycosidic torsion angles ϕ and ψ are usually deduced from interresidue NOE measurements between protons adjacent to the linkage (e.g., H1 and H4′, Scheme 1), although NOEs between more remote proton pairs may also be used if observable.[1] In general, however, the number of observable NOEs sensitive to ϕ and ψ is limited, especially in smaller structures, and thus linkage conformation is often difficult to determine in this manner, especially if flexibility is suspected.[2] The latter problem stems from nonlinear averaging of the NOE in which conformations containing the more potent relaxation pathways (i.e., shorter internuclear distances) are more heavily weighted in the measurement.

The above problems necessitate the development of alternate NMR parameters as additional conformational constraints in oligosaccharides, and $^{13}C-^1H$ and $^{13}C-^{13}C$ spin coupling constants have attracted attention in this regard.[3] In a typical *O*-glycosidic linkage, six trans-glycoside couplings involving carbon are available; for example, in the generic [1→4] linkage shown in Scheme 1, three couplings ($^3J_{C4',H1}$, $^2J_{C1,C4'}$, $^3J_{C2,C4'}$) are sensitive to ϕ, and three ($^3J_{C1,H4'}$, $^3J_{C1,C3'}$, $^3J_{C1,C5'}$) are sensitive to ψ. Thus, a reasonable degree of redundancy is present with which to assess each C−O torsion in the linkage. Measurements of $^3J_{COCH}$ values across these linkages have become routine in recent years, even in natural abundance molecules. In contrast, trans-*O*-glycosidic $^2J_{COC}$ and $^3J_{COCC}$ values are rarely obtained, despite their potential advantages, mainly because their measurement requires ^{13}C-enrichment and their dependencies on molecular structure are poorly understood. Recent experimental and theoretical studies of $^2J_{COC}$ and $^3J_{COCC}$ in saccharides have begun to define the latter dependencies, thus providing a firmer basis for their application in oligosaccharide structure determination.[4] Despite this recent progress, however, a full understanding of $^2J_{COC}$ and $^3J_{COCC}$ in saccharides remains elusive; indeed, despite several reports of Karplus relationships,[5] the same can be claimed for $^3J_{COCH}$. While model compounds have been used extensively in experimental studies to establish correlations between $^2J_{COC}$, $^3J_{COCC}$, and molecular structure,[4a−e]

Scheme 1

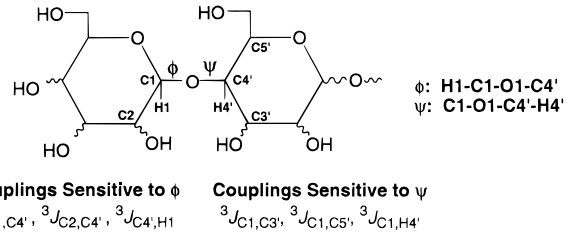

* Corresponding author.
[†] Department of Chemistry and Biochemistry.
[‡] Radiation Laboratory.

(1) Homans, S. W. *Prog. NMR Spectrosc.* **1990**, *22*, 55−81.
(2) (a) Cumming, D. A.; Carver, J. P. *Biochemistry* **1987**, *26*, 6664−6676. (b) Yan, Z.-Y.; Bush, C. A. *Biopolymers* **1990**, *29*, 799−811.
(3) (a) Rutherford, T. J.; Partridge, J.; Weller, C. T.; Homans, S. W. *Biochemistry* **1993**, *32*, 12715−12724. (b) Gagnaire, D. Y.; Nardin, R.; Taravel, F. R.; Vignon, M. R. *Nouv. J. Chem.* **1977**, *1*, 423−430. (c) Nunez, H. A.; Barker, R. *Biochemistry* **1980**, *19*, 489−495. (d) Hayes, M. L.; Serianni, A. S.; Barker, R. *Carbohydr. Res.* **1982**, *100*, 87−101. (e) Landersjo, C.; Stenutz, R.; Widmalm, G. *J. Am. Chem. Soc.* **1997**, *119*, 8695−8698.

10.1021/ja984384t CCC: $18.00
Published on Web 10/13/1999

it is clear that this traditional approach has significant limitations. Model compounds closely mimicking actual molecules are restricted in number, are often difficult to label with ^{13}C, and sometimes yield anomalous couplings due to the presence of structural strain. Thus, studies of *J* coupling would benefit greatly from reliable computational tools that permit their accurate calculation in the actual molecule, or in a closely related structure, under investigation. These theoretical methods could also be applied to test predictions made via experiment and/or provide new complementary data on which to derive firmer structure/*J* coupling correlations.

Recent investigations have shown that density functional theory (DFT) can be used to calculate reliable J_{CH} and J_{CC} values in carbohydrates without the need for scaling;[4d,6] DFT-computed J_{CH} and J_{CC} values were estimated to be within 5% and 10%, respectively, of experimental values. In the present work, we extend this approach to four disaccharide mimics, **1**−**4**, in order to obtain optimized molecular geometries, from which trans-*O*-glycosidic $^3J_{COCH}$ and $^3J_{COCC}$ values were calculated as a function of glycosidic torsion angles. Computed couplings are compared to the experimental coupling data reported previously[4d] and confirm, modify, and/or extend prior correlations between $^3J_{COCH}$ and $^3J_{COCC}$ values and molecular structure in saccharides.

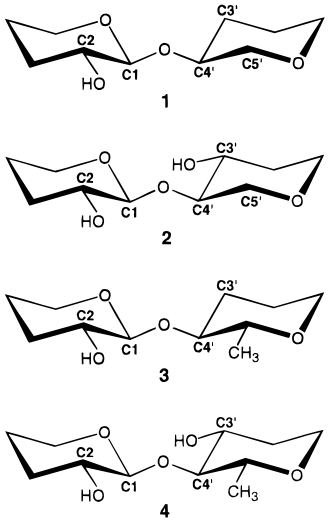

Computational Methods

Ab Initio Molecular Orbital Calculations. Ab initio molecular orbital calculations were performed with a modified[7] version of the Gaussian 94 suite of programs[8] on disaccharide mimics **1**−**4**. Electron correlation effects were treated by means of DFT. The standard B3LYP functional, from Becke,[9] was used in all calculations. This functional comprises both local[10] and nonlocal[11] exchange contributions and contains terms accounting for local[12] and nonlocal[13] correlation corrections.

Geometric Optimization and Calculations of $^{13}C-^1H$ and $^{13}C-^{13}C$ Spin Coupling Constants. Geometric optimizations were conducted with the B3LYP functional and the standard split-valence 6-31G* basis set.[14] In this report, the ϕ glycosidic torsion angle is defined as H1−C1−O1−C4′, and the ψ glycosidic torsion angle is defined as C1−O1−C4′−H4′ (Scheme 1).

$^{13}C-^1H$ and $^{13}C-^{13}C$ spin coupling constants in optimized structures were obtained by finite field (Fermi contact) double perturbation theory[15] calculations at the B3LYP level using a basis set previously constructed for similar systems.[7] Appropriate values for the perturbing fields imposed on the coupled nuclei were chosen to ensure sufficient numerical precision while still allowing a satisfactory low-order finite difference representation of the effect of the perturbation. Only the Fermi contact component of each coupling constant was considered due to the dominant relationship of this term in *J* values involving carbon and hydrogen in saturated systems.

Results and Discussion

General Considerations. The principal aim of this investigation is to extend the DFT method, applied previously to monosaccharides,[4d,6a,b] to studies of the structures of, and J_{CH} and J_{CC} couplings in, disaccharides. To minimize the complexity of the calculations, structures **1**−**4** were chosen as disaccharide mimics. These model disaccharides possess substituents in the vicinity of the *O*-glycosidic linkage which are expected to mimic those found in authentic β-[1→4] linkages. These substituents include a C2 hydroxyl group (OH2), a C3′ hydroxyl group (OH3′), and/or a C5′ methyl group ($CH_3$5′), with OH2 a common substituent in all structures. Systematic incorporation of OH3′ and $CH_3$5′ was expected to provide information on the effect of pyranosyl ring substitution in the vicinity of the linkage on linkage conformation. We first examine the structural parameters and energies of geometrically optimized **1**−**4**. These optimized structures are then used to calculate $^{13}C-^1H$ and $^{13}C-^{13}C$ spin couplings across the *O*-glycosidic linkage, and resulting calculated couplings are compared to experimental couplings.[4d,5] The latter data were inherently restricted by the number of useful model compounds available for study and/or by structural uncertainties due to conformational averaging in solution, and thus the theoretical treatment was expected to improve *J* coupling/structure correlations.

In earlier work, we showed that trends in computed J_{CC} and J_{CH} could be predicted reliably using ab initio molecular orbital methods at the HF level of theory,[16] but that *J* values computed in this fashion were not quantitative due to the neglect of electron correlation in HF theory. To address this limitation, scaling factors were developed to adjust the HF calculations to those that include correlation effects (quadratic configuration interaction). DFT[17a] represents an alternative approach that treats

(4) (a) Church, T.; Carmichael, I.; Serianni, A. S. *Carbohydr. Res.* **1996**, *280*, 177−186. (b) Serianni, A. S.; Bondo, P. B.; Zajicek, J. *J. Magn. Reson. Ser. B* **1996**, *112*, 69−74. (c) Zhao, S.; Bondo, G.; Zajicek, J.; Serianni, A. S. *Carbohydr. Res.* **1998**, *309*, 145−152. (d) Bose, B.; Zhao, S.; Stenutz, R.; Cloran, F.; Bondo, P.; Bondo, G.; Hertz, B.; Carmichael, I.; Serianni, A. S. *J. Am. Chem. Soc.* **1998**, *120*, 11158−11173. (e) Milton, M. J.; Harris, R.; Probert, M. A.; Field, R. A.; Homans, S. W. *Glycobiology* **1998**, *8*, 147−153. (f) Xu, Q.; Bush, C. A. *Carbohydr. Res.* **1998**, *306*, 335−339.

(5) (a) Tvaroska, I.; Hricovini, H.; Petrakova, E. *Carbohydr. Res.* **1989**, *189*, 359−362. (b) Mulloy, B.; Frenkiel, T. A.; Davies, D. B. *Carbohydr. Res.* **1988**, *184*, 39−46.

(6) (a) Cloran, F.; Carmichael, I.; Serianni, A. S. *J. Phys. Chem. A* **1999**, *103*, 3783−3795. (b) Hricovini, M.; Malkina, O. L.; Bizik, F.; Nagy, L. T.; Malkin, V. G. *J. Phys. Chem. A* **1997**, *101*, 9756−9762. (c) Stahl, M.; Schopfer, U.; Frenking, G.; Hoffmann, R. W. *J. Org. Chem.* **1997**, *62*, 3702−3704.

(7) Carmichael, I. *J. Phys. Chem.* **1993**, *97*, 1789−1792.

(8) Frisch, M. J.; Trucks, G. W.; Schlegel, H. B.; Gill, P. M. W.; Johnson, B. G.; Robb, M. A.; Cheeseman, J. R.; Keith, T.; Petersson, G. A.; Montgomery, J. A.; Raghavachari, K.; Al-Laham, M. A.; Zakrzewski, V. G.; Ortiz, J. V.; Foresman, J. B.; Peng, C. Y.; Ayala, P. Y.; Chen, W.; Wong, M. W.; Andres, J. L.; Replogle, E. S.; Gomperts, R.; Martin, R. L.; Fox, D. J.; Binkley, J. S.; Defrees, D. J.; Baker, J.; Stewart, J. P.; Head-Gordon, M.; Gonzalez, C.; Pople, J. A. *Gaussian 94*; Gaussian, Inc.: Pittsburgh, PA, 1995.

(9) Becke, A. D. *J. Chem. Phys.* **1993**, *98*, 5648−5652.

(10) Slater, J. C. *The Self-Consistent Field for Molecules and Solids*; McGraw-Hill: New York, 1974.

(11) Becke, A. D. *ACS Symp. Ser.* **1989**, *394*, 165.

(12) Vosko, S. H.; Wilk, L.; Nusair, M. *Can. J. Phys.* **1980**, *58*, 1200.

(13) Lee, C.; Yang, W.; Parr, R. G. *Phys. Rev. B* **1988**, *37*, 785.

(14) Hehre, W. J.; Ditchfield, R.; Pople, J. A. *J. Chem. Phys.* **1972**, *56*, 2257−2261.

(15) Kowalewski, J.; Laaksonen, A.; Roos, B.; Siegbahn, P. *J. Chem. Phys.* **1979**, *71*, 2896−2902.

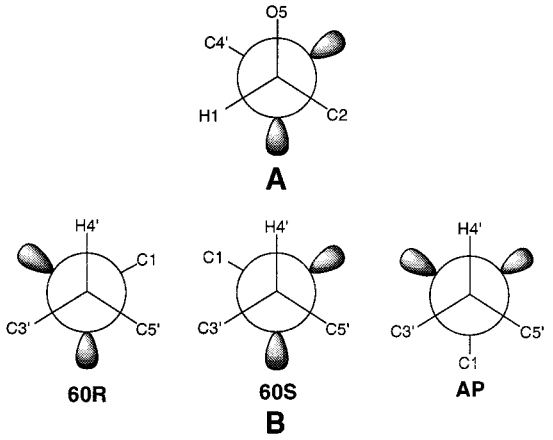

Figure 1. Newman projections defining the initial values of ϕ (A) and ψ (B) in the disaccharide mimics **1**−**4**.

correlation effects explicitly at a computational cost not much greater than that of HF calculations. It has been shown that the DFT treatment provides accurate predictions of structural parameters[17b] and nearly quantitative $^{13}C-^{13}C$ and $^{13}C-^{1}H$ spin couplings in a wide range of bonding environments without the need for scaling.[6] Consequently, the DFT approach was adopted to optimize geometries and calculate *J* values in **1**−**4**.

DFT-Optimized Geometries of 1−4. In all calculations on **1**−**4**, the constituent pyranosyl rings were in the $^4C_1$ conformation. All structures contain a β-[1→4] linkage, and the C1−O1 and C4′−O1 bonds are equatorial. For each structure, the initial C1−O1 torsion (ϕ, defined as H1−C1−O1−C4′; Scheme 1) was chosen to optimize the exoanomeric effect[18] (i.e., C2 *anti* to C4′) (Figure 1A), and the initial C2−O2 torsion was chosen arbitrarily, with OH2 *anti* to C1. In **2**, the C3′−O3′ bond is equatorial, and the initial C3′−O3′ torsion was chosen to orient OH3′ *anti* to C2′, whereas in **3**, the $CH_3$5′ substituent is equatorial. Similar geometric constraints for OH3′ and $CH_3$5′ were imposed in **4**. In **1**−**4**, the initial O1−C4′ torsion angle (ψ, defined as C1−O1−C4′−H4′; Scheme 1) was chosen to place substituents in a staggered orientation (Figure 1B); it was presumed that three local minima (stable geometries) are associated with these staggered rotamers, which are defined as 60R, 60S, and AP (Figure 1B). Geometric optimizations were performed with the B3LYP functional and a polarized split-valence basis set (6-31G*).

For **1**, geometric optimizations proceeded smoothly, generating three unique structures approximating the initial three rotamers (Figures 2 and 3); structural parameters and conformational energies for these rotamers are found in Table 1. In contrast, only *two* unique structures (60S and AP) were obtained upon optimization of the three starting rotamers of **2**−**4** (Figures 4 and 5). In these three cases, the 60R rotamer converted spontaneously to the 60S rotamer. Structural parameters and conformational energies for the 60S and AP rotamers of **2**−**4** are found in Tables 2 and 3, respectively.

In the optimized geometries of **1**−**4**, the AP rotamer is 2.4−3.2 kcal/mol higher in energy than the corresponding 60S geometry. In **1**, the 60R rotamer is 0.1 kcal/mol higher in energy than the 60S form. Thus, in all cases, the 60S form is the most stable rotamer. In the optimized 60R and 60S geometries of **1**,

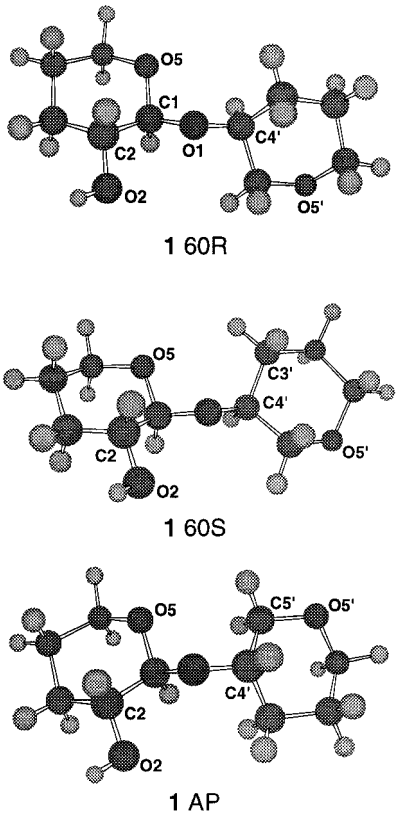

Figure 2. Three-dimensional representations of the optimized structures of **1** 60R, **1** 60S, and **1** AP determined by DFT (B3LYP/6-31G*).

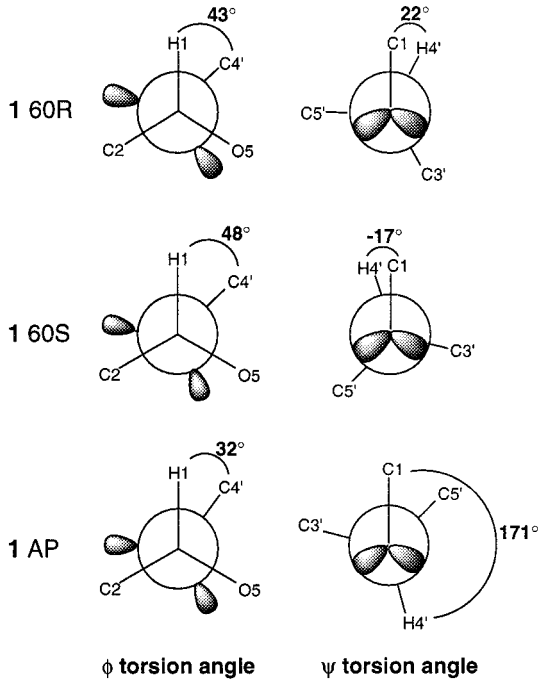

Figure 3. Newman projections showing optimized ϕ and ψ values for **1** 60R, **1** 60S, and **1** AP determined by DFT (B3LYP/6-31G*).

(16) (a) Carmichael, I.; Chipman, D. M.; Podlasek, C. A.; Serianni, A. S. *J. Am. Chem. Soc.* **1993**, *115*, 10863−10870. (b) Podlasek, C. A.; Stripe, W. A.; Carmichael, I.; Shang, M.; Basu, B.; Serianni, A. S. *J. Am. Chem. Soc.* **1996**, *118*, 1413−1425. (c) Church, T. J.; Carmichael, I.; Serianni, A. S. *J. Am. Chem. Soc.* **1997**, *119*, 8946−8964. (d) Serianni, A. S.; Wu, J.; Carmichael, I. *J. Am. Chem. Soc.* **1995**, *117*, 8645−8650.

(17) (a) Malkin, V. G.; Malkina, O. L.; Eriksson, L. A.; Salahub, D. R. In *Modern Density Functional Theory: A Tool for Chemistry*, Seminario, J. M., Politzer, P., Eds.; Elsevier Science B.V.: Amsterdam, The Netherlands, 1995; Vol. 2, pp 273−347. (b) Bauschlicher, C. W., Jr.; Partridge, H. *Chem. Phys. Lett.* **1995**, *240*, 533−40.

(18) (a) Lemieux, R. U. *Pure Appl. Chem.* **1971**, *25*, 527−548. (b) Lemieux, R. U.; Koto, S.; Voisin, D. In *Anomeric Effect: Origin and Consequences*; Szarek, W. A., Horton, D., Eds.; ACS Symposium Series 87; American Chemical Society: Washington, DC, 1979; pp 17−29. (c) Praly, J.-P.; Lemieux, R. U. *Can. J. Chem.* **1987**, *65*, 213−223.

Table 1. Selected Structural Parameters and Conformational Energies in **1**

parameter	60R	60S	AP	parameter	60R	60S	AP	parameter	60R	60S	AP
					Bond Lengths[a]						
C1−C2	1.5309	1.5317	1.5326	C4′−C5′	1.5347	1.5333	1.5379	C5−H5 (eq)	1.0939	1.0939	1.0939
C2−C3	1.5375	1.5372	1.5365	C1′−O5′	1.4237	1.4238	1.4230	C1′−H1′ (ax)	1.1046	1.1046	1.1050
C3−C4	1.5350	1.5347	1.5342	C4′−O1	1.4338	1.4333	1.4337	C1′−H1′ (eq)	1.0944	1.0944	1.0944
C4−C5	1.5288	1.5286	1.5285	C5′−O5′	1.4218	1.4206	1.4237	C2′−H2′ (ax)	1.0980	1.0981	1.0979
C1−O1	1.3871	1.3842	1.3875	C1−H1	1.1068	1.1076	1.1044	C2′−H2′ (eq)	1.0976	1.0977	1.0976
C2−O2	1.4229	1.4225	1.4238	C2−H2	1.1012	1.1012	1.1010	C3′−H3′ (ax)	1.0991	1.0990	1.0987
C1−O5	1.4254	1.4272	1.4274	C3−H3 (ax)	1.0989	1.0989	1.0990	C3′−H3′ (eq)	1.0956	1.0943	1.0955
C5−O5	1.4238	1.4243	1.4245	C3−H3 (eq)	1.0986	1.0986	1.0986	C4′−H4′	1.0972	1.0992	1.0958
C1′−C2′	1.5308	1.5299	1.5305	C4−H4 (ax)	1.0974	1.0974	1.0974	C5′−H5′ (ax)	1.1030	1.1034	1.1019
C2′−C3′	1.5375	1.5378	1.5383	C4−H4 (eq)	1.0973	1.0973	1.0973	C5′−H5′ (eq)	1.0942	1.0935	1.0923
C3′−C4′	1.5278	1.5314	1.5340	C5−H5 (ax)	1.1042	1.1042	1.1045				
					Bond Angles[b]						
C1−O1−C4′	115.4	116.3	118.9	O1−C1−C2	110.6	108.8	108.4	O1−C4′−C5′	109.4	107.0	114.1
C5−O5−C1	113.2	113.3	113.5	O1−C1−H1	111.5	111.0	112.2	O1−C4′−H4′	109.9	109.7	103.3
O5−C1−O1	107.8	108.5	107.8	O1−C4′−C3′	108.6	111.2	113.0				
					Bond Torsions[b]						
O5−C1−O1−C4′	−76.2	−72.0	−88.3	C1′−O5′−C5′−C4′	61.4	60.9	62.0	O5′−C5′−C4′−O1	−176.1	−176.9	173.9
C1−C2−C3−C4	−50.5	−50.9	−50.5	C1−C2−O2−H	177.8	178.1	175.8	C1−O1−C4′−H4′	21.7	−17.1	170.7
C1−O5−C5−C4	62.9	62.8	62.7	C1−O1−C4′−C3′	141.3	104.5	−72.3	H1−C1−O1−C4′	43.4	47.5	31.9
C1′−C2′−C3′−C4′	−51.3	−51.1	−51.3	C1−O1−C4′−C5′	−98.5	−134.9	55.0	C2−C1−O1−C4′	163.8	167.8	152.0
				energy[c]	0.1	0.0	2.6				

[a] In angstroms. [b] In degrees. [c] In kcal/mol relative to 60S.

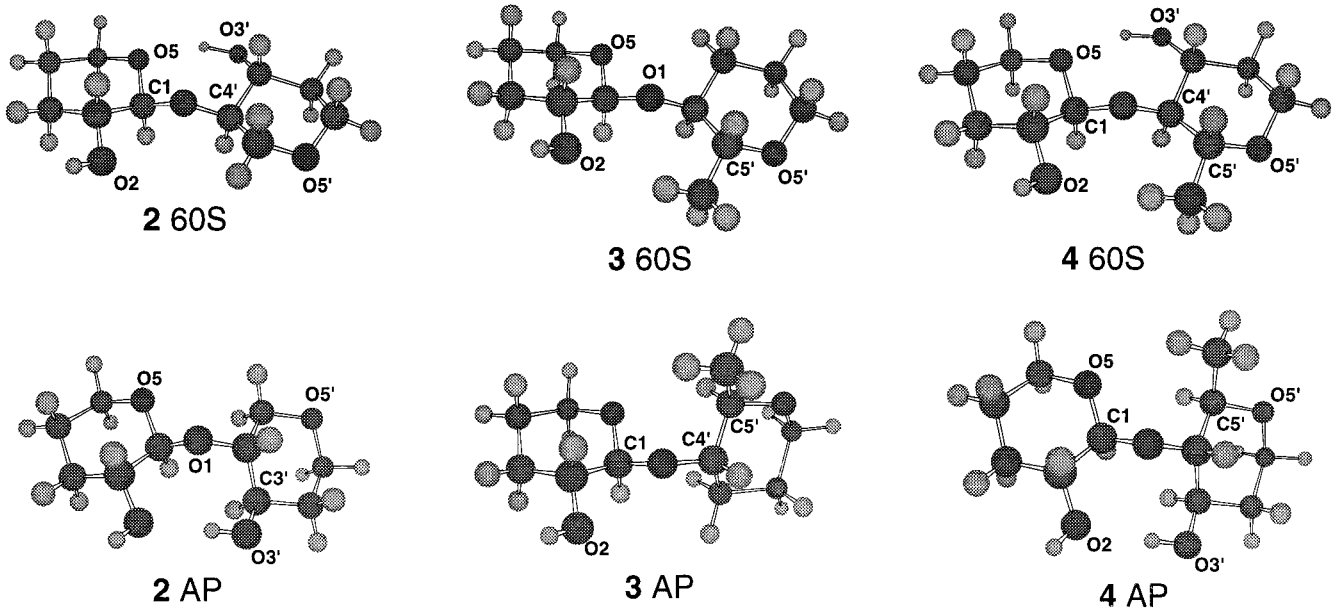

Figure 4. Three-dimensional representations of the geometrically optimized structures of **2** 60S, **2** AP, **3** 60S, **3** AP, **4** 60S, and **4** AP determined by DFT (B3LYP/6-31G*).

ψ differs by only ~40° (Figure 3). The initial 60R and 60S geometries of **1** appear to approach a common geometry, but slight steric and/or stereoelectronic factors apparently prevent a 60R → 60S transition.

In **2** and **4**, an equatorial hydroxyl group is present on C3′, and geometric optimization yielded proximal orientations of OH3′ and O5 in 60S forms and of OH3′ and O2 in AP forms (Figure 4). In **2** 60S and **4** 60S, the O3′−O5 inter-oxygen distances were 2.830 and 2.827 Å, respectively, while in **2** AP and **4** AP, the O3′−O2 inter-oxygen distances were 2.983 and 2.944 Å, respectively (Tables 2 and 3). These distances suggest the presence of hydrogen bonding between these functional groups. Additional evidence of H bonding derives from the O−H···O angles, which range from 157°−163° (Tables 2 and 3). In idealized hydrogen bonding of this type, this angle approaches 180°, and the inter-oxygen distance is ~2.8 Å. This interresidue H bonding may have important implications for the conformational properties of **2** and **4**, as discussed below.

In **2**−**4**, only two unique rotamers were obtained upon geometric optimization of the three staggered rotamers about ψ. The 60R geometry converged to the 60S geometry in each case. In contrast, unique geometries were obtained for the 60R, 60S, and AP rotamers of **1**. These results suggest that driving forces in **2**−**4** exist that destabilize the 60R geometry and/or stabilize the 60S geometry. In **2**, interresidue hydrogen bonding (O3′−H′···O5) is probably the driving force in the conversion of 60R to 60S. In the initial 60R geometry, OH3′ is relatively far from the O5 lone pairs, but as optimization proceeds, hydrogen bonding occurs and presumably drives the rotation of ψ over the eclipsed geometry into the 60S regime, where H bonding between OH3′ and O5 is stronger. Interestingly, a similar conversion from 60R to 60S is observed for **3**, but in

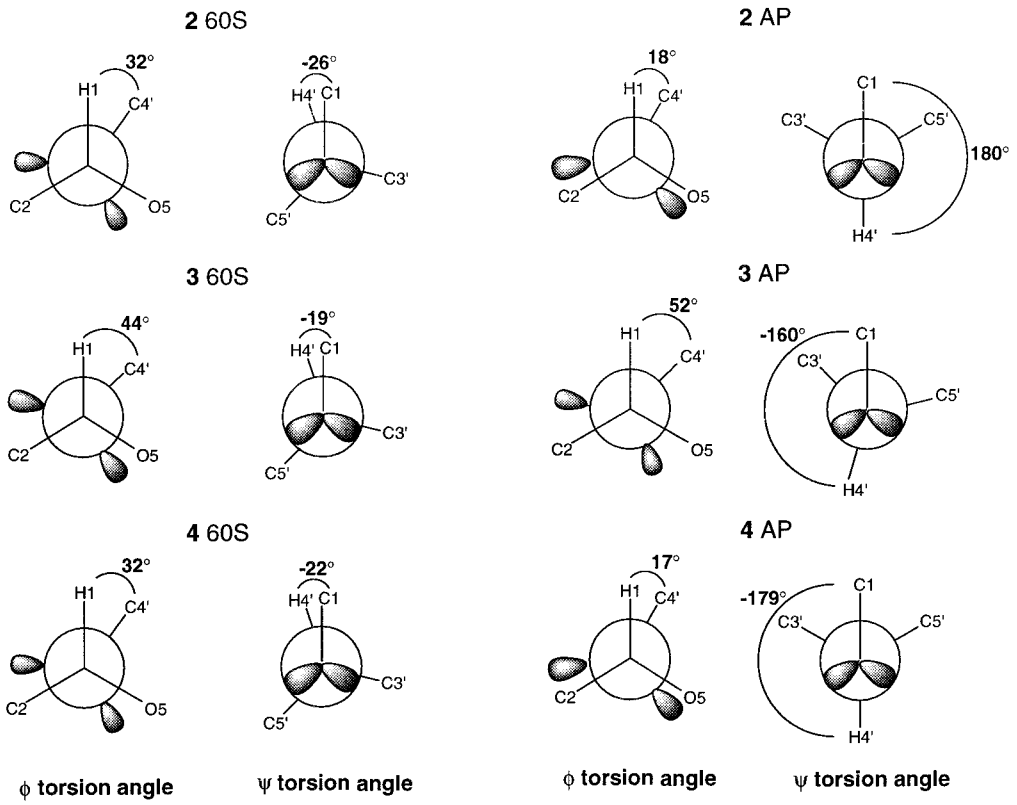

Figure 5. Newman projections showing optimized ϕ and ψ values for **2** 60S, **2** AP, **3** 60S, **3** AP, **4** 60S, and **4** AP determined by DFT (B3LYP/6-31G*).

Table 2. Selected Structural Parameters and Conformational Energies in 60S Rotamer of **2**−**4**

parameter	**2** 60S	**3** 60S	**4** 60S	parameter	**2** 60S	**3** 60S	**4** 60S	parameter	**2** 60S	**3** 60S	**4** 60S
				Bond Lengths[a]							
C1−C2	1.5312	1.5321	1.5323	C5′−CH_3		1.5210	1.5217	C5−H5 (ax)	1.1024	1.1042	1.1024
C2−C3	1.5371	1.5370	1.5372	C1′−O5′	1.4248	1.4221	1.4226	C5−H5 (eq)	1.0933	1.0939	1.0932
C3−C4	1.5346	1.5350	1.5348	C3′−O3′	1.4144		1.4152	C1′−H1′ (ax)	1.1042	1.1045	1.1041
C4−C5	1.5272	1.5286	1.5268	C4′−O1	1.4371	1.4345	1.4407	C1′−H1′ (eq)	1.0938	1.0948	1.0941
C1−O1	1.3815	1.3834	1.3809	C5′−O5′	1.4168	1.4291	1.4256	C2′−H2′ (ax)	1.0969	1.0982	1.0969
C2−O2	1.4220	1.4241	1.4235	C1−H1	1.1045	1.1071	1.1044	C2′−H2′ (eq)	1.0966	1.0977	1.0967
C1−O5	1.4378	1.4271	1.4374	C2−H2	1.1011	1.1008	1.1007	C3′−H3′ (ax)	1.1053	1.0988	1.1051
C5−O5	1.4308	1.4243	1.4305	C3−H3 (ax)	1.0987	1.0985	1.0987	C3′−H3′ (eq)		1.0943	
C1′−C2′	1.5288	1.5288	1.5269	C3−H3 (eq)	1.0983	1.0985	1.0982	C4′−H4′	1.0991	1.1004	1.0996
C2′−C3′	1.5308	1.5359	1.5285	C4−H4 (ax)	1.0973	1.0974	1.0973	C5′−H5′ (ax)	1.1034	1.1049	1.1047
C3′−C4′	1.5352	1.5323	1.5371	C4−H4 (eq)	1.0970	1.0973	1.0970	C5′−H5′ (eq)	1.0930		
C4′−C5′	1.5345	1.5406	1.5429								
				Bond Angles[b]							
C1−O1−C4′	118.3	116.9	118.7	O1−C1−C2	109.2	108.6	109.2	O1−C4′−C5′	106.0	107.3	106.5
C5−O5−C1	113.6	113.3	113.7	O1−C1−H1	111.3	111.1	111.4	O1−C4′−H4′	109.7	109.6	109.7
O5−C1−O1	109.6	108.5	108.1	O1−C4′−C3′	111.9	110.6	110.5				
				Bond Torsions[b]							
O5−C1−O1−C4′	−87.9	−75.9	−87.7	C1−C2−O2−H	176.9	175.0	173.3	C1−O1−C4′−H4′	−25.5	−19.4	−22.1
C1−C2−C3−C4	−51.4	−50.6	−51.2	C1−O1−C4′−C3′	95.2	102.0	97.8	C4′−O1−C1−H1	31.7	43.8	32.0
C1−O5−C5−C4	63.0	62.9	63.3	C1−O1−C4′−C5′	−143.8	−136.7	−140.4	C2−C1−O1−C4′	152.9	163.9	153.4
C1′−C2′−C3′−C4′	−51.3	−51.1	−50.9	C1′−O5′−C5′−CH_3		−175.8	−176.9	O5′−C5′−C4′−O1	−177.4	−175.8	−174.3
C1′−O5′−C5′−C4′	60.5	60.7	59.8	C2′−C3′−O3′−H	174.3		174.3				
				Interatomic Distances[a]							
O3′−O5	2.8304		2.8274	O3′−H	0.9776		0.9773	O5−H(O3′)	1.9045		1.8999
				Interatomic Angles[b]							
				O3′−H−O5	157.0		157.4				
				energy[c]	0.0	0.0	0.0				

[a] In angstroms. [b] In degrees. [c] In kcal/mol relative to 60S.

this case H bonding cannot be implicated, and thus steric effects are presumably involved. In **3** 60R, steric interactions are encountered between $CH_3$5′ and H1 which are stronger than those encountered in **3** 60S. These interactions apparently induce rotation to the more stable 60S geometry, where the methyl group is further displaced from H1. Thus, it appears that hydrogen bonding and steric effects independently facilitate the conversion of 60R to 60S in **2**−**4** and behave as *reinforcing*

Table 3. Selected Structural Parameters and Conformational Energies in AP Rotamers of **2**−**4**

parameter	**2** AP	**3** AP	**4** AP	parameter	**2** AP	**3** AP	**4** AP	parameter	**2** AP	**3** AP	**4** AP
				Bond Lengths[a]							
C1−C2	1.5331	1.5337	1.5340	C5′−CH_3		1.5198	1.5213	C5−H5 (ax)	1.1042	1.1040	1.1040
C2−C3	1.5329	1.5373	1.5333	C1′−O5′	1.4248	1.4202	1.4227	C5−H5 (eq)	1.0935	1.0938	1.0935
C3−C4	1.5359	1.5342	1.5355	C3′−O3′	1.4122		1.4125	C1′−H1′ (ax)	1.1046	1.1047	1.1046
C4−C5	1.5294	1.5279	1.5291	C4′−O1	1.4346	1.4384	1.4395	C1′−H1′ (eq)	1.0938	1.0948	1.0941
C1−O1	1.3901	1.3853	1.3900	C5′−O5′	1.4211	1.4339	1.4298	C2′−H2′ (ax)	1.0968	1.0976	1.0968
C2−O2	1.4331	1.4228	1.4329	C1−H1	1.1034	1.1037	1.1030	C2′−H2′ (eq)	1.0967	1.0977	1.0967
C1−O5	1.4203	1.4293	1.4223	C2−H2	1.0994	1.1010	1.0993	C3′−H3′ (ax)	1.1057	1.0985	1.1056
C5−O5	1.4261	1.4252	1.4263	C3−H3 (ax)	1.0988	1.0988	1.0987	C3′−H3′ (eq)		1.0967	
C1′−C2′	1.5317	1.5302	1.5291	C3−H3 (eq)	1.0982	1.0986	1.0982	C4′−H4′	1.0946	1.0972	1.0953
C2′−C3′	1.5295	1.5376	1.5277	C4−H4 (ax)	1.0973	1.0974	1.0973	C5′−H5′ (ax)	1.1035	1.1006	1.1054
C3′−C4′	1.5364	1.5329	1.5383	C4−H4 (eq)	1.0970	1.0973	1.0970	C5′−H5′ (eq)	1.0928		
C4′−C5′	1.5353	1.5454	1.5432								
				Bond Angles[b]							
C1−O1−C4′	119.4	120.1	119.9	O1−C1−C2	107.9	107.9	110.4	O1−C4′−C5′	113.7	112.6	114.1
C5−O5−C1	113.1	113.5	113.1	O1−C1−H1	112.3	112.0	109.2	O1−C4′−H4′	103.2	103.2	102.9
O5−C1−O1	107.8	108.8	107.9	O1−C4′−C3′	112.7	114.9	111.9				
				Bond Torsions[b]							
O5−C1−O1−C4′	−102.8	−68.7	−104.0	C1−C2−O2−H	170.8	176.7	169.7	C1−O1−C4′−H4′	179.6	−159.6	−178.9
C1−C2−C3−C4	−50.8	−50.6	−50.9	C1−O1−C4′−C3′	−64.8	−41.7	−63.9	C4′−O1−C1−H1	17.6	51.9	16.5
C1−O5−C5−C4	61.9	62.9	62.3	C1−O1−C4′−C5′	62.6	85.9	64.6	C2−C1−O1−C4′	137.3	171.6	136.6
C1′−C2′−C3′−C4′	−53.2	−52.2	−52.8	C1′−O5′−C5′−CH_3		−175.0	−177.8	O5′−C5′−C4′−O1	173.8	171.6	175.8
C1′−O5′−C5′−C4′	60.1	62.3	59.4	C2′−C3′−O3′−H	−177.8		−177.0				
				Interatomic Distances[a]							
O3′−O2	2.9828		2.9443	O3′−H	0.9773		0.9774	O2−H(O3′)	2.0373		1.9981
				Interatomic Angles[b]							
				O3′−H−O2	162.6		162.3				
				energy[c]	2.4	3.2	2.8				

[a] In angstroms. [b] In degrees. [c] In kcal/mol relative to 60S.

Table 4. ϕ and ψ Torsion Angles (Degrees) in AP Rotamers of **1**−**4**

	1	**2**	**3**	**4**
ϕ	31.9	17.6	51.9	16.5
ψ	170.7	179.6	200.4	181.1

Table 5. ϕ and ψ Torsion Angles (Degrees) in the 60S Rotamers of **1**−**4**

	1	**2**	**3**	**4**
ϕ	47.5 (43.4)[a]	31.7	43.8	32.0
ψ	−17.1 (21.7)[a]	−25.5	−19.4	−22.1

[a] Values in parentheses are **1** 60R torsion angles.

interactions in this conversion. Evidence for this synergy derives from the behavior of **4**, where both OH3′ and $CH_3$5′ are present. In this case, again only the 60S geometry is obtained upon optimization of initial 60R and 60S geometries.

The AP geometries of **1**−**4** show very similar structures about the glycosidic linkage (Figures 3 and 5). However, some differences in glycosidic torsion angles are observed and warrant discussion. Table 4 gives ϕ and ψ torsion angles in the AP forms. In the AP geometries, ϕ varies from ∼18° to 52°. In structures where interresidue hydrogen bonding between OH3′ and O2 is present (**2** and **4**), ϕ is reduced (17.6° and 16.5°, respectively) from the idealized torsion angle of ∼60°, where the exoanomeric effect might be maximized. This deviation is probably caused by the interplay between interresidue hydrogen bonding and the exoanomeric effect. The reduction of ϕ in **2** and **4** is somewhat relieved in **1** and **3** (31.9° and 51.9°, respectively), where OH3′ is absent. Steric effects caused by the aglycon lead to an adjustment of ϕ (31.9°) in **1** from the idealized value of ∼60°. In **3**, the $CH_3$5′ group may encounter weak steric interactions with the O5 lone pairs, thereby altering ϕ to reduce this repulsion. The ψ torsion angle remains relatively constant in the AP geometries, ranging from ∼171° to 200°. The ψ value in **3** (200.4°) is somewhat enhanced; this probably reflects the need for the sterically demanding methyl group to distance itself from the O5 lone pairs. Apparently, rotation about ϕ is less favored to relieve this steric stress than that about ψ, presumably because stereoelectronic forces controlling ϕ are relatively strong. The steric influence of the methyl group in determining ϕ and ψ is considered to be mild in comparison to the influence of interresidue H bonding, since the values of ϕ and ψ in **4** are more similar to those in **2** than to those in **3**.

The 60S structures in **1**−**4** are also very similar in their geometries about the glycosidic linkage, but differences in the torsion angles ϕ and ψ occur (Table 5). For ϕ in **1**−**4**, values are 32°−48° are observed, with ϕ in **2** and **4** ∼12° less than that in **3**. Variations in ϕ from the idealized value of 60° in **1** may be due to steric effects induced by the large aglycon group. A significant change in ϕ arises when OH3′ is present on **2** and **4**. As in the AP rotamer, ϕ is reduced in order to accommodate interresidue H bonding, in this case between OH3′ and O5. As pointed out for the AP rotamer, an interplay between hydrogen bonding and the exoanomeric effect probably exists to dictate a potential energy minimum. The ψ torsion angle also remains relatively constant in the 60S geometries (∼ −17° to −26°). Steric effects induced by the presence of the aglycon results in a ψ value of ∼ −20° for all geometries. It is more difficult to assess the individual effects of the aglycon substituents on ψ since the trends are not as well defined.

It should be noted that the addition of a methyl group in **3**, which exerts minor effects on ϕ and ψ relative to **1** in the 60S form (Table 5), is sufficient to destabilize 60R (or stabilize 60S). This fact suggests that the barrier of interconversion between 60R and 60S may be sufficiently low in **3** that only small steric effects introduced in the 60R geometry are required to facilitate the transition to the more favored 60S geometry; H bonding,

Table 6. Calculated Trans-*O*-glycoside Vicinal $^{13}C-^{1}H$ and $^{13}C-^{13}C$ Spin Couplings[a] in **1**−**4**

disaccharide	$^{3}J_{C1,O1,C4',H4'}$	$^{3}J_{C4',O1,C1,H1}$	$^{3}J_{C1,O1,C4',C3'}$	$^{3}J_{C1,O1,C4',C5'}$	$^{3}J_{C2,C1,O1,C4'}$
1 AP	7.9 (170.7°)[b]	4.3 (31.9°)	0.5 (−72.3°)	1.9 (55.0°)	3.7 (152.0°)
1 60S	5.8 (−17.1°)	4.1 (47.5°)	−0.1 (104.5°)	3.7 (−134.9°)	4.2 (167.8°)
1 60R	5.6 (21.7°)	4.0 (43.4°)	2.4 (141.3°)	−0.1 (−98.5°)	3.8 (163.8°)
2 AP	8.6 (179.6°)	4.4 (17.6°)	1.1 (−64.8°)	1.5 (62.6°)	2.6 (137.3°)
2 60S	5.2 (−25.5°)	5.1 (31.7°)	−0.3 (95.2°)	4.9 (143.8°)	3.8 (152.9°)
3 AP	8.1 (−159.6°)	2.3 (51.9°)	3.5 (−41.7°)	−0.4 (85.9°)	4.1 (171.6°)
3 60S	5.8 (−19.4°)	4.3 (43.8°)	−0.2 (102.0°)	4.0 (−136.7°)	4.1 (163.9°)
4 AP	8.6 (−178.9°)	4.2 (16.5°)	1.3 (−63.9°)	1.4 (64.6°)	2.5 (136.6°)
4 60S	5.4 (−22.1°)	4.9 (32.0°)	−0.2 (97.8°)	4.3 (−140.4°)	3.7 (153.4°)

[a] In hertz; *uncorrected* computed values. These values were corrected by +5% and −10%, respectively, prior to plotting in Figures 6 and 7. [b] Values in parentheses are corresponding torsion angles between the coupled nuclei.

Table 7. Calculated Trans-*O*-glycoside Vicinal $^{13}C-^{1}H$ and $^{13}C-^{13}C$ Spin Couplings[a] in ψ-Constrained Geometries[b] of **1**

disaccharide	$^{3}J_{C1,O1,C4',H4'}$	$^{3}J_{C4',O1,C1,H1}$	$^{3}J_{C1,O1,C4',C3'}$	$^{3}J_{C1,O1,C4',C5'}$	$^{3}J_{C2,C1,O1,C4'}$
1 60	1.4 (60°)[c]	2.0 (54.9°)	4.4 (177.6°)	1.8 (−62.3°)	3.4 (175.0°)
1 80	1.0 (80°)	1.7 (58.1°)	4.3 (−163.0°)	3.8 (−42.0°)	3.4 (177.9°)
1 110	0.5 (110°)	2.6 (47.6°)	2.6 (−133.5°)	5.7 (−10.3°)	3.8 (167.5°)
1 130	2.8 (130°)	3.0 (43.8°)	0.8 (−112.3°)	5.3 (12.9°)	3.9 (163.4°)
1 150	5.8 (150°)	3.7 (38.1°)	−0.2 (−97.1°)	4.0 (34.9°)	3.9 (157.8°)

[a] In hertz; *uncorrected* computed values. These values were corrected by +5% and −10%, respectively, prior to plotting in Figures 6 and 7. [b] Constrained ψ angles at values of 60°, 80°, 110°, 130°, and 150°. [c] Values in parentheses are corresponding torsion angles between the coupled nuclei.

therefore, is not required to stimulate the 60R → 60S transition. When an OH3′ group is added (to give **4**), the transition from 60R to 60S is enhanced because, as ψ rotates from an idealized 60° (perfectly staggered) to 21.7° (60R optimization of **1**), hydrogen bonding between OH3′ and O5 becomes possible, and optimization of this H bonding induces further rotation. As ψ rotates, any positive changes in energy due to a transition through an eclipsed state are compensated by the strengthening of the H bond.

Trans-*O*-glycosidic $^{13}C-^{1}H$ and $^{13}C-^{13}C$ Spin Coupling Constants in 1−4. The geometrically optimized **1**−**4** were used to calculate trans-*O*-glycosidic $^{3}J_{COCH}$ and $^{3}J_{COCC}$ values for comparison to coupling behavior reported previously, obtained using experimental methods.[4d,5] Since one of the glycosidic torsion angles (ϕ, H1−C1−O1−C4′) was constrained by the exoanomeric effect and the second (C1−O1−C4′−H4′) was limited to extreme torsion angles (∼20° and ∼160°−180°), additional information was needed to explore the torsional dependence of $^{3}J_{COCH}$ for dihedral angles in the range 60°−150°. Additional geometric optimizations were therefore performed on **1**, with ψ held constant at 60°, 80°, 110°, 130°, and 150° (structural data not shown). It is important to appreciate that these constrained structures are not energetically stable, i.e., they do not fall in local potential energy minima. This 60°−150° range of torsions was chosen instead of the −60° to −150° range to reduce the possibility of steric interactions adversely affecting the molecular geometry. In previous DFT analyses of 2-deoxy-β-D-*erythro*-pentofuranose,[6a] model aldopyranosyl rings, and methyl aldopyranosides,[4d,6b] it was estimated that computed J_{CH} and J_{CC} values differed in magnitude from those measured experimentally by approximately −5% and +10%, respectively. Consequently, in this study, +5% and −10% correction factors were applied to the computed J_{CH} and J_{CC} data, respectively. J_{CH} and J_{CC} coupling data (uncorrected) in the fully optimized geometries of **1**−**4**, and in the ψ-constrained geometries of **1**, are found in Tables 6 and 7.

Trans-*O*-glycosidic Three-Bond $^{13}C-^{1}H$ Couplings. In **1**−**4**, trans-*O*-glycosidic $^{3}J_{C1,O1,C4',H4'}$ and $^{3}J_{C4',O1,C1,H1}$ values were calculated and compared to experimental data reported previously.[5] The latter data indicated a Karplus dependency for $^{3}J_{COCH}$, but a complete correlation between *J* and dihedral angle

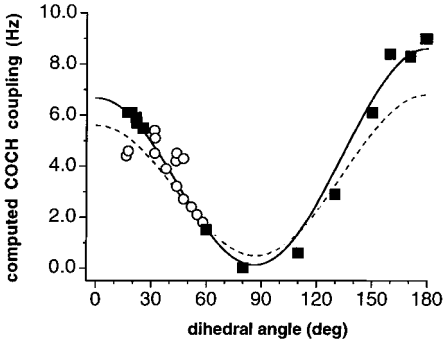

Figure 6. Computed trans-*O*-glycoside $^{3}J_{COCH}$ values (corrected) as a function of dihedral angle θ in **1**−**4** using the DFT method ([5s2p1d|2s] basis set) at the B3LYP/6-31G* geometries. The dashed line is the experimental Karplus relationship (eq 3),[5a] and the solid line is the computed relationship (eq 2). ■, $^{3}J_{C1,H4'}$ data; ○, $^{3}J_{C4',H1}$ data.

θ was not achievable due to the limited availability of appropriate model compounds. A least-squares fitting of the computed $^{3}J_{COCH}$ values (Tables 6 and 7) was made to the following generalized Karplus equation (eq 1):

$$^{3}J_{COCH} = A\cos^{2}\theta + B\cos\theta + C \qquad (1)$$

This fitting gave eq 2, which can be compared to the Karplus equation proposed previously by Tvaroska and co-workers,[5a] obtained using experimental methods (eq 3).

$$^{3}J_{COCH} = 7.49\cos^{2}\theta - 0.96\cos\theta + 0.15 \qquad (2)$$

$$^{3}J_{COCH} = 5.7\cos^{2}\theta - 0.6\cos\theta + 0.5 \qquad (3)$$

Figure 6 is a plot of the computed $^{3}J_{COCH}$ data, the Karplus fit to these computed data (eq 2), and the experimentally determined Karplus equation (eq 3). The agreement between the computed and experimental couplings as a function of dihedral angle θ is very good. The principal difference between the two data sets is the larger calculated couplings at the extreme dihedral angles. Factors such as solvation, basis set limitations, and the small set of geometries and structures studied (e.g., one

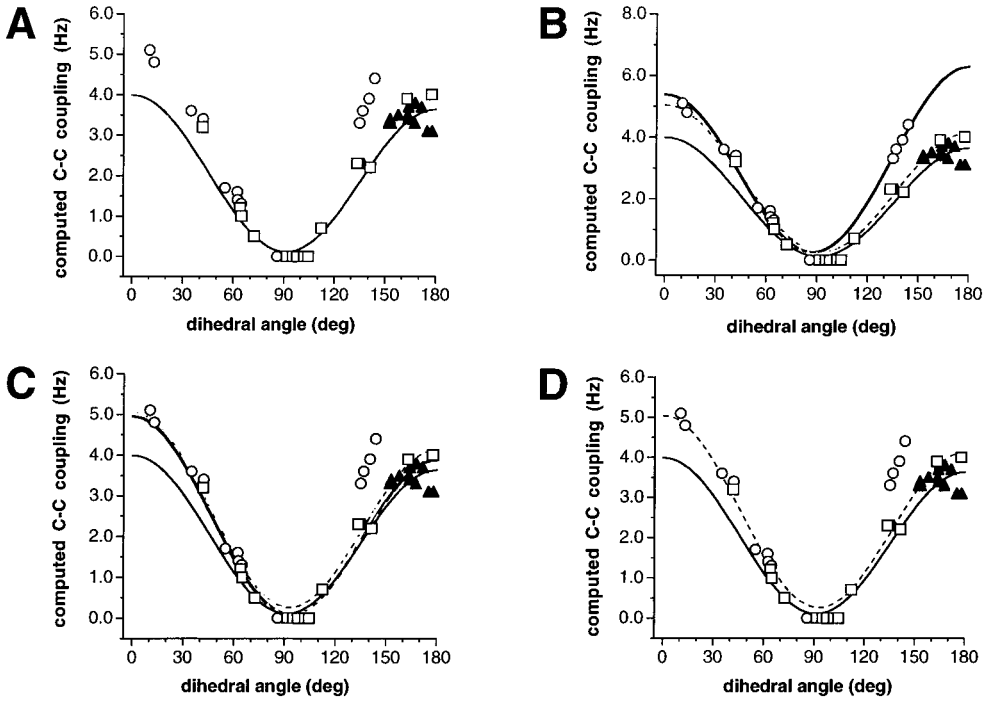

Figure 7. Computed trans-*O*-glycoside $^3J_{COCC}$ values (corrected) as a function of dihedral angle θ in **1**−**4** plotted with (A) the experimental Karplus relationship (eq 4; solid line);[4d] (B) eq 4 (solid line), eq 6 (thick line), and eq 8 (dashed line); (C) eq 4 (solid line), eq 7 (thick line), and eq 8 (dashed line); and (D) eq 4 (solid line) and eq 8 (dashed line). *J* couplings were calculated by the DFT method ([5s2p1d|2s] basis set) at the B3LYP/6-31G* geometries. Absolute values of dihedral angles were used in these plots. □, $^3J_{C1,C3'}$ data; ○, $^3J_{C1,C5'}$ data; ▲, $^3J_{C2,C4'}$ data.

rotamer of ϕ, one type of glycosidic linkage) may be, in part, responsible for the deviations from the experimental curve, although some experimental reassessment of couplings for $\theta = 0°$ and 180° may be warranted to establish whether some of the deviation is real.

Trans-*O*-glycosidic Three-Bond $^{13}C-^{13}C$ Couplings. In **1**−**4**, trans-*O*-glycosidic $^3J_{C1,O1,C4',C3'}$, $^3J_{C1,O1,C4',C5'}$, and $^3J_{C2,C1,O1,C4'}$ values were calculated as a function of dihedral angle θ, and the dependency was compared to that reported previously using experimental approaches.[4d] In the experimentally derived curve, relatively few data points for $\theta = 0°-100°$ were available, and the present computational data were obtained, in part, to rectify this problem. The calculated $^3J_{COCC}$ values listed in Tables 6 and 7 are consistent with those reported experimentally. In prior experimental work,[4d] two Karplus equations were proposed for C−O−C−C coupling pathways; one included the possibility of asymmetric maxima at $\theta = 0°$ and 180° (eq 4), and a second assumed identical maxima (eq 5).

$$^3J_{COCC} = 3.70\cos^2\theta + 0.18\cos\theta + 0.11 \quad (4)$$

$$^3J_{COCC} = 3.49\cos^2\theta + 0.16 \quad (5)$$

An important caveat in the development of eqs 4 and 5 was that couplings enhanced by in-plane terminal oxygens were excluded from the parametrization. We expected that, with the increased data for $\theta = 0°-100°$, a more precise assessment of relative amplitudes at $\theta = 0°$ and 180° would be possible, thereby permitting a justifiable distinction between eqs 4 and 5 and a better quantitation of the in-plane effects of terminal electronegative substituents.

A plot of the computed $^3J_{COCC}$ versus θ superimposed on the experimentally derived Karplus curve (eq 4) (Figure 7A) shows that the computed couplings are consistent in magnitude with experimental data. Interestingly, in the dihedral angle range $\theta = 135°-145°$ for the C1−O1−C4′−C5′ pathway, computed couplings lie significantly *above* the experimental curve; if $^3J_{COCC}$ were determined solely by θ, dihedrals closer to 180° would be required to produce these larger couplings. Inspection of the C1−O1−C4′−C5′ pathway shows that, in some linkage geometries, O5′ lies in the C1−O1−C4′−C5′ plane, and based on the reported effects of terminal electronegative substituents on $^3J_{COCC}$ magnitude,[4d] these geometries are expected to enhance $^3J_{C1,C5'}$. This enhancement is substantiated in these calculations. Furthermore, the computed couplings for $\theta = 0°-60°$ are *larger* than predicted by the experimental data. We attribute this to the lack of experimental couplings in this dihedral range, which made this region of the curve less certain and led to the proposal of two potential Karplus equations (eqs 4 and 5) to treat the data. The DFT-calculated couplings for $\theta < 100°$ suggest that eq 4 may be the more accurate relationship, that is, one where couplings at 0° are somewhat larger than those at 180°, at least in the absence of in-plane effects.

Due to the uniqueness of the C1−O1−C4′−C5′ pathway, where in-plane effects can operate, three parametrized Karplus curves were developed through a least-squares fitting: one parametrization uses only $^3J_{C1,C5'}$ data (eq 6), one uses only data from $^3J_{C1,C3'}$ and $^3J_{C2,C4'}$ (eq 7), and one uses all coupling data (eq 8).

$$^3J_{COCC} = 6.17\cos^2\theta - 0.51\cos\theta + 0.30 \quad (6)$$

$$^3J_{COCC} = 4.96\cos^2\theta + 0.63\cos\theta - 0.01 \quad (7)$$

$$^3J_{COCC} = 4.96\cos^2\theta + 0.52\cos\theta + 0.18 \quad (8)$$

Plots of eqs 4, 6, and 8, and of eqs 4, 7, and 8, superimposed on the computed data, are shown in Figure 7B and 7C, respectively. A comparison of these figures shows the displacement of the $^3J_{C1,C5'}$ values caused by in-plane effects. Furthermore, the experimentally parameterized curve appears more consistent with the parametrization derived from $^3J_{C1,C3'}$ and

$^3J_{C2,C4'}$ data (eq 7) than from $^3J_{C1,C5'}$ data (eq 6), as expected, since the former was determined by excluding coupling data where in-plane effects were suspected. A plot of eqs 4 and 8 superimposed on the computed data is shown in Figure 7D. A comparison of eq 8 (all three pathways) with eqs 6 and 7 shows that the former is more consistent with eq 7. This finding is probably due to the clustering of the $^3J_{C2,C4'}$ data for $\theta = \sim 135°-180°$, which is caused by the dependence of $^3J_{C2,C4'}$ on ϕ. This torsion angle is highly conserved due to the choice of the initial torsion angle in the calculations. The high concentration of points in this region (135°−180°) and the absence of in-plane effects on $^3J_{C2,C4'}$ make eq 8 very similar to eq 7.

Although differences are observed between the experimental parametrization of $^3J_{COCC}$ and the computational parametrizations (eqs 6−8) for dihedral angles of 0°−60°, the magnitudes of the DFT-calculated $^3J_{COCC}$ values and their dependency on θ are remarkably consistent with experimental values, suggesting that, despite the known limitations of the computational approach used herein, the DFT method can be expected to yield accurate coupling trends and nearly quantitative predictions of $^3J_{COCC}$ values in saccharides.

Conclusions

This investigation provides new theoretical treatments of $^3J_{COCH}$ and $^3J_{COCC}$ in carbohydrates which should facilitate their interpretation in oligosaccharide conformational analysis. Previous experimental investigations of J_{CH} and J_{CC} in saccharides depended heavily on the use of simple model compounds to establish correlations between J magnitude and molecular structure.[4d,5] The present theoretical calculations on disaccharide mimics provide a test of the coupling predictions drawn from these prior experimental measurements and of the accuracy and reliability of J calculations in saccharides. The results confirm and extend recent correlations[4d] between $^3J_{COCC}$ and C−O−C−C dihedral angle. Except for the region which lacked sufficient experimental data points for reliable fitting, the computationally parameterized Karplus curve for $^3J_{COCC}$ determined herein is in excellent agreement with the experimental curve.[4d] In addition, the appearance of in-plane effects of terminal electronegative substituents in the computed trans-*O*-glycosidic $^3J_{C1,C5'}$ values is consistent with experimental findings where these effects were first revealed.[4d] The computationally parameterized $^3J_{COCH}$ Karplus curve derived herein is also in good agreement with those derived experimentally.[5] Larger computed $^3J_{COCH}$ values were found, however, at the extreme dihedral angles (∼0°−20° and 160°−180°), suggesting that some refinement of the experimental curve may be needed.

While the accuracy of the theoretical method used in this study is remarkable, it should be appreciated that only a small subset of disaccharide linkage geometries was examined, specifically those containing β-[1→4] linkages where ϕ was initially set to optimize the exoanomeric effect (C4′ *gauche* to O5 and H1). In the present study, we were limited by the considerable computation times required to conduct geometric optimizations and scalar coupling calculations on these moderately large molecules, although a sufficient range of molecular torsion angles was inspected to generate Karplus curves of high quality for both $^3J_{COCH}$ and $^3J_{COCC}$. Future studies of β-[1→4] disaccharide mimics should examine other initial values of ϕ, while other linkage types (e.g., α-[1→4]) and ring substitution patterns (e.g., *N*-substitution) remain to be explored. Such studies will provide additional tests of previous experimental predictions of how these variables affect Karplus dependencies. Nevertheless, given the high degree of accuracy of the DFT method in predicting J_{CH} and J_{CC} values in saccharides and the ongoing improvements in computational theory and computer hardware, it is likely that future studies of J couplings in saccharides and related molecules may rely less heavily on generalized Karplus curves derived solely from experimental studies of model compounds. Instead, specific J coupling/structure relationships will be derived computationally for specific coupling pathways in the molecule under consideration, thus minimizing the need for generalized curves and the inherent uncertainties that accompany their use.

Scheme 2

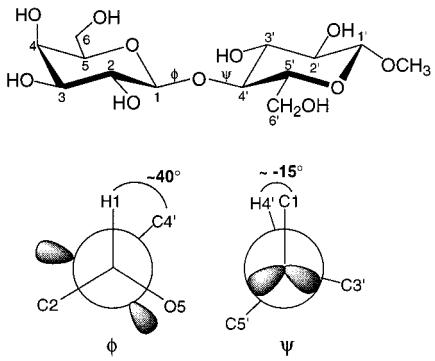

For the lowest energy rotamers of **1**−**4**, computed ϕ and ψ values of 31.7°−47.5° and −17.1° to −25.5° were observed. These values are in good agreement with experimental values reported for the β-[1→4]-linked disaccharide, methyl β-lactoside, in solution ($\phi = 40°$, $\psi = -15°$; Scheme 2) based on an analysis of $^3J_{COCH}$ and $^3J_{COCC}$ values,[3d,4d] and in a recent crystal structure ($\phi = 33°$, $\psi = -41°$).[19a] These prior studies also indicated that methyl β-lactoside exists in one highly favored conformation in aqueous solution with respect to *O*-glycosidic linkage. In this simple case, the preferred linkage geometries deduced from the optimized disaccharide mimics are validated, but a more complex treatment will be needed for disaccharides that exist in multiple conformations in solution. Furthermore, the glycosidic torsion angles reported by Hirotsu and Shimada for several disaccharides using crystallographic data are also consistent with the optimized torsion angles for the lowest energy geometries.[19b] Even though these crystal structures, and that recently obtained for methyl β-lactoside,[19a] may not be completely representative of conformation in solution, the consistency of the DFT-optimized geometries with experimental results provides a reasonable validation of the method and encourages further applications to oligosaccharides. Present efforts are directed at experimental and computational studies of a range of biologically relevant ^{13}C-labeled di- and trisaccharides, where different linkage conformations are expected. These investigations will enlarge the present database of $^3J_{COCH}$ and $^3J_{COCC}$ values across *O*-glycosidic linkages and permit a more comprehensive test of their utility as conformational constraints. In the latter regard, a theoretical, generalized treatment of the extent to which redundant J_{CH} and J_{CC} values across these linkages can be used to determine the degree of linkage flexibility would be valuable.

Acknowledgment. This work was supported by a grant from Omicron Biochemicals, Inc. of South Bend, IN, and by the Office of Basic Energy Sciences of the United States Department of Energy. This is Document No. NDRL-4113 from the Notre Dame Radiation Laboratory.

JA984384T

(19) (a) Stenutz, R.; Shang, M.; Serianni, A. S. *Acta Crystallogr.*, in press. (b) Hirotsu, K.; Shimada, A. *Bull. Chem. Soc. Jpn.* **1974**, *47*, 1872−1879.